2025年度　11）SCOSTEP Visiting Scholar (SVS) Program (in ISEE)　目次詳細

2025　11）SCOSTEP Visiting Scholar (SVS) Program in ISEE
List

6 件

＊所属・職名は2026年3月現在

＊Affiliation and Department displayed are current as of March 2026.

研究代表者 Principal Investigator	所属機関* Affiliation	所属部局* Department	職名* Job title	研究課題名 Project Title	頁 Page	備考 Remarks
Amrutha	Indian Institute of Geomagnetism, India		graduate-course student	High Frequency Magnetosonic Waves and the Radiation Belt Electrons	360	
B Gayathri	Indian Institute of Geomagnetism, India	Dynamical and Electrodynamical Coupling of the Atmosphere-ionosphere system using radio and optical techniques (DECA)	graduate-course student	Investigation of Seeding of postmidnight irregularities in the South Asian sector	363	
Kristyna Drastichova	Faculty of Mathematics and Physics, Charles University, Prague, Czech Republic		graduate-course student	Power line harmonic radiation observed by the PWING network	365	
Thomas Lheureux	CNRS/ Toulouse University, France		graduate-course student	Thermospheric and Ionospheric Perturbations at Mid-Latitudes during Solar Maximum : Implications for Space Weather.	371	
Manar Gamal	Egypt-Japan University for Science and Technology(E-JUST), Egypt	Space Environment Lab (SERL)	graduate-course student	Forbush Decreases at Mid-Latitudes: Simulating Cosmic Ray Flux Variations with PHITS and Geant4	374	
Arthur Gauthier	DLR (Deutsches Zentrum für Luft und Raumfahrt), Germany		graduate-course student	Fabry Perot observations of the thermospheric wind and its response to a geomagnetic storm event	376	

High Frequency Magnetosonic Waves and the Radiation Belt Electrons

Amrutha
Research Scholar
Indian Institute of Geomagnetism, India

The primary goal of this visit was to study the high frequency magnetosonic (MS) waves and their interaction with electrons by harnessing MS wave events from satellite data and studying their electron pitch angle distribution concurrent to the wave event to identify the interaction pattern and connect it with resonance effects.

To begin with, a MS wave event observed by the ARASE satellite with frequencies between 10 and 12 Hz was studied, which occurred on 10 February 2018, as reported by *Asamura et al. (2021)*. The magnetic field measurements were taken from the MGF instrument, and electron pitch angle data was obtained from the low, medium, and high-energy electron sensors (LEP-e, MEP-e, and HEP-e). The wave mode was identified as MS by determining the wave normal angle (WNA) and ellipticity using the Singular Value Decomposition (SVD) technique. MS waves have WNA close to 90° and ellipticity around 0, indicating linear polarization. The root mean squared (RMS) wave amplitude is calculated by integrating over the frequencies from 10 to 12 Hz. The electron resonance energies were then calculated using the parallel wave number derived from the theoretical dispersion relation developed by *Amrutha et al. (2024)*. Based on these resonance energies, the corresponding electron pitch angle distributions were investigated.

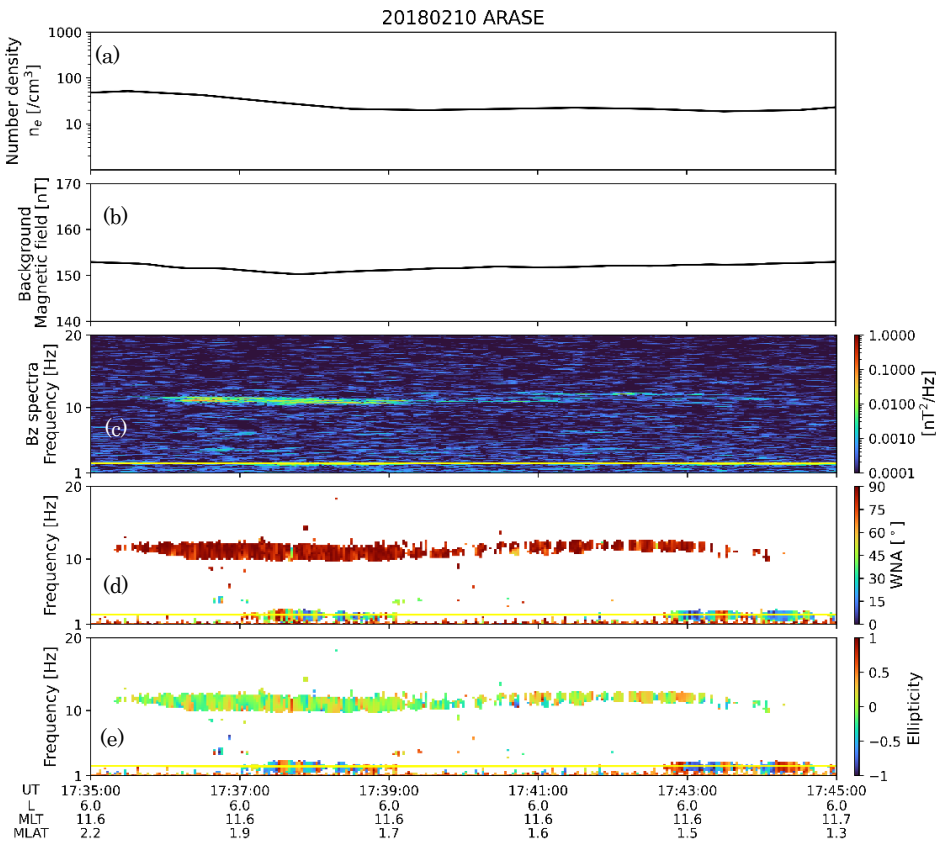

Figure 1: MS wave event of 10 February, 2018 observed by the ARASE satellite. (a) Electron density profile calculated by HFA. (b) Ambient magnetic field calculated using the magnetic field vector from MGF. (c) Power spectral density of the wave magnetic field from MGF. (d) WNA and (e) ellipticity calculated using the SVD technique. Yellow solid line in panels (c), (d), and (e) denotes the local proton cyclotron frequency.

The average number density and the background magnetic field calculated based on the data from HFA and MGF (Figure 1) is taken as input parameters to the theoretical model to calculate the minimum resonant energy of electrons using the relativistic electron cyclotron resonance condition given by

$$\omega - k_{\parallel} v_{\parallel} = -n\Omega_{ce}/\gamma,$$

where ω is the wave frequency, $k_{\parallel}$ is the parallel wavevector, Ω_{ce} is the electron cyclotron frequency, and γ is the Lorentz factor *(Horne et al., 2007)*. Landau resonance condition is given by $n = 0$, while $n = 1$ and $n = 2$ gives cyclotron resonance condition of order 1 and 2, respectively. For the MS wave event of 10 February 2018, the minimum Landau, first and second order cyclotron resonant energies calculated for different propagation angles are given in Figure 2. It is observed that the Landau resonant energy is highly dependent on the propagation angle.

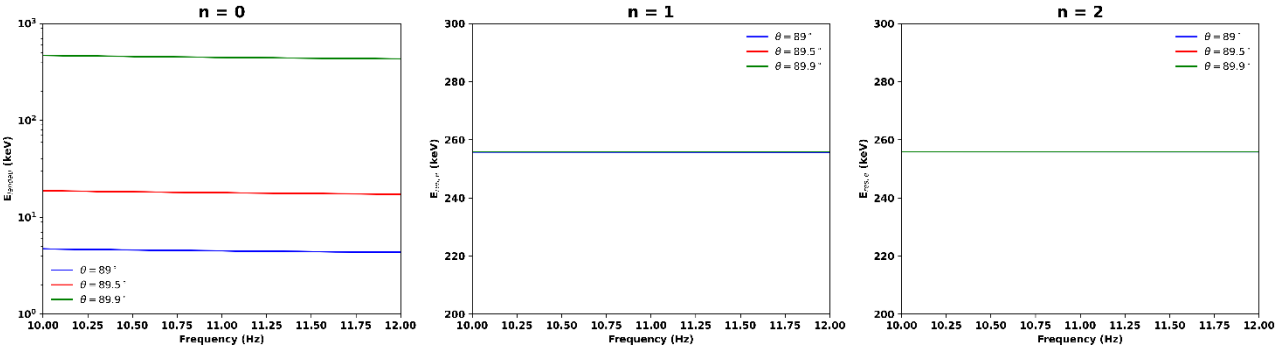

Figure 2: (a) Landau, (b) First order cyclotron and (c) second order cyclotron resonant energies of electron interacting with MS waves of frequency 10 to 12 Hz calculated using the theoretical model mentioned in *Amrutha et al. (2024)* for different propagation angles, indicated by the legends.

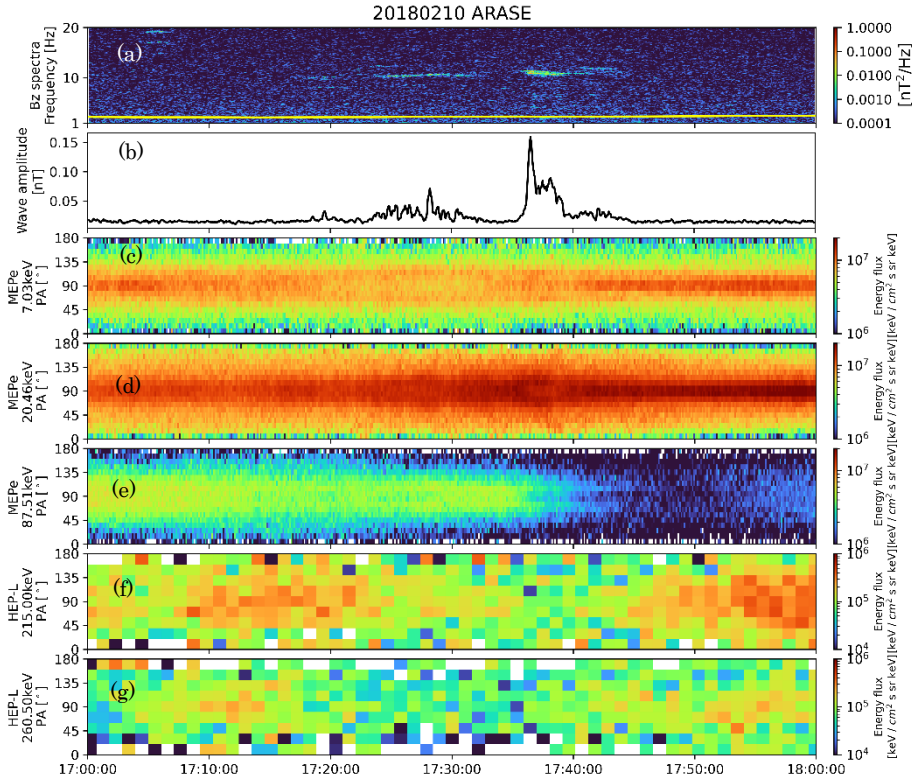

Figure 3: (a) Power spectral density of the wave magnetic field from MGF. (b) RMS wave amplitude for frequencies from 10 to 12 Hz. (c - e) Pitch angle distribution of medium energy electrons (7.03 – 87.51 keV) measured by MEPe. (e and f) Pitch angle distribution of high energy electrons (215 and 260.50 keV) measured by HEPe.

From Figure 3, it is evident that there is a decrease in the energy flux of 90° pitch angle, medium energy electrons coinciding with the RMS amplitude peaks of the MS waves. The maximum wave amplitude reaches up to 0.15 nT. These energy ranges fall around the minimum Landau resonant energy values corresponding to propagation angles 80° to 89.5° . This flux decrease may be also due to other wave modes present at the same time. Therefore, further analysis is required to draw any conclusions.

During the course of this project, several important insights were gained. The timescale of electron interactions with MS waves is relatively long and noticeable changes in electron behavior are more likely to occur during high amplitude wave events *(Horne et al., 2007; Maldonado et al., 2016)*. Additionally, because one component of the search-coil magnetometer of the ARASE satellite has not been working since October 2018, the availability of WNA measurements above a few tens of hertz is limited, making it difficult to clearly distinguish between MS waves and whistlers. To address this problem, we plan to extend our study by including events observed by the RBSP satellites as well.

The period of stay at ISEE was **90 days**, from **July 1st to September 27th, 2025**. Along with the main research topic, other related works were covered during this time:

- Analysis of MS and EMIC wave events over the entire ARASE observation period up to the most recent data (March 2017 to October 2024), to build a database of low frequency wave events (from 1 Hz to 1 kHz) for future studies.
- Identification of some events showing the simultaneous occurrence of multiple harmonics of MS waves together with high-frequency EMIC waves (figures not included). These findings form the foundation for testing the hypothesis proposed by *Asamura et al. (2021)* using multiple events.

- Got the opportunity to present two months of work at the ARASE annual meeting held at the University of Tokyo, as well as to participate and present in various other meetings at the institute.

Even though the original aim of the work at ISEE could not be fully completed, the progress made provides a strong foundation for future publications. Moreover, this opportunity has given valuable experience and insight into topics that completes my Ph.D. thesis. My sincere thanks are due to Professor Yoshizumi Miyoshi for his guidance, and to ISEE and SCOSTEP for providing financial support for this work.

References:

1. Horne, R. B., R. M. Thorne, S. A. Glauert, N. P. Meredith, D. Pokhotelov, and O. Santolík (2007), Electron acceleration in the Van Allen radiation belts by fast magnetosonic waves, Geophys. Res. Lett., 34, L17107, doi:10.1029/2007GL030267.
2. Maldonado, A. A., L. Chen, S. G. Claudepierre, J. Bortnik, R. M. Thorne, and H. Spence (2016), Electron butterfly distribution modulation by magnetosonic waves, Geophys. Res. Lett., 43, 3051–3059, doi:10.1002/2016GL068161.
3. Asamura, K., Shoji, M., Miyoshi, Y., Kasahara, Y., Kasaba, Y., Kumamoto, A., Tsuchiya, F., Matsuda, S., Matsuoka, A., Teramoto, M., Kazama, Y., and Shinohara, I (2021), Cross-Energy Couplings from Magnetosonic Waves to Electromagnetic Ion Cyclotron Waves through Cold Ion Heating inside the Plasmasphere, Phys. Rev. Lett., 127, 245101, doi:10.1103/PhysRevLett.127.245101.
4. Amrutha, S. V. Singh, K. C. Barik, and G. S. Lakhina (2024), Magnetosonic Waves Excited by Maxwellian Ring Protons in Space Plasma Environment, 972 (188), doi: 10.3847/1538-4357/ad65cb.

Investigation of Seeding of postmidnight irregularities in the South Asian sector

B Gayathri
Research scholar
Indian Institute of Geomagnetism (IIG)

Our work mainly focuses on investigating the seeding of postmidnight irregularities near the magnetic equator using the 47 MHz Equatorial Atmosphere Radar (EAR) in West Sumatra, Indonesia (0.20ºS, 100.32ºE; dip latitude 10.36ºN). Simultaneous Total electron content (TEC) perturbations associated with these irregularities were observed by satellites from north of the GPS receivers. We found that the wavy TEC perturbations were associated with the occurrence of Field Aligned Irregularities (FAIs) observed on 11 August 2019. Furthermore, using detrended total electron content (DTEC) two-dimensional (2D) maps, we observed the propagation of these wavy structures in the meridional (northeastward) direction, which is an unusual scenario, as FAIs and medium-scale traveling ionospheric disturbances (MSTIDs) typically propagate southwestward. The electrodynamics of these wavy structures require further investigation.

Dataset used for the study

The EAR radar, which is sensitive to 3-meter-scale irregularities, was used to investigate the postmidnight irregularities during the summer months of the low solar activity year 2019. Additionally, TEC data were obtained from the GPS receiver network in Sumatra, Indonesia, known as Sumatran GPS Array (SuGAr). TEC perturbations are derived by subtracting a 1-hour running average from the slant TEC. We used five SuGAr receivers located north of the EAR site, operated by Nagoya University. DTEC maps were employed to study the spatiotemporal evolution of TEC perturbations, using data from approximately 115 receivers.

Results

The TEC wavy perturbations associated with the FAIs observed near the magnetic equator

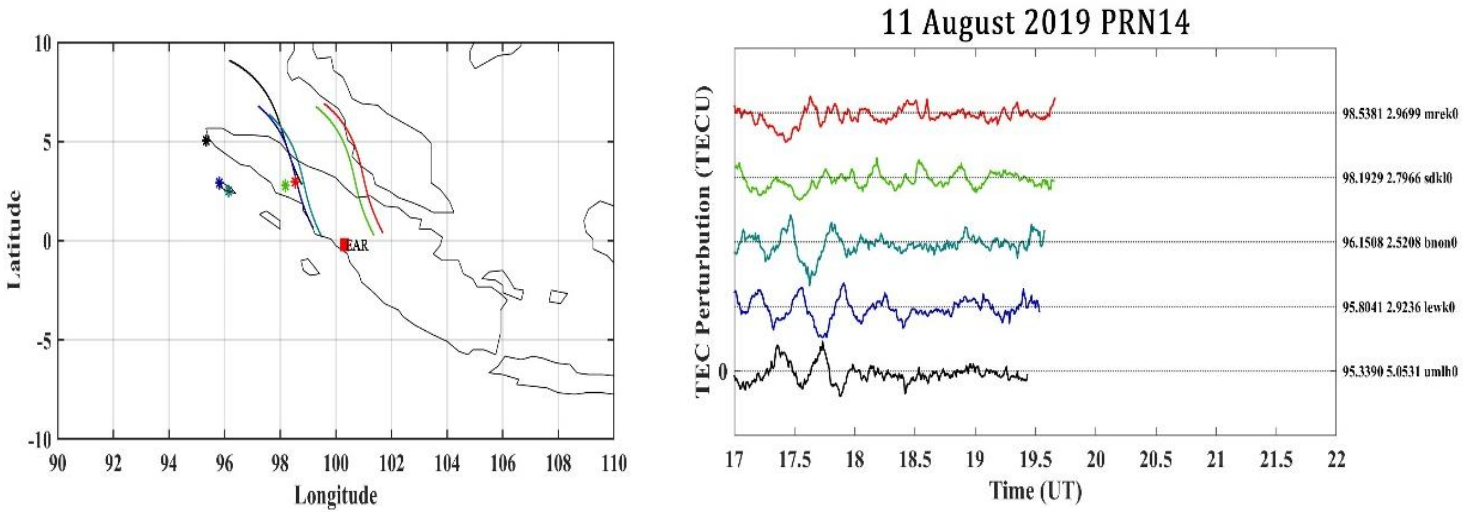

Figure 1: (a) shows the satellite passes observed from the northern receivers located near the EAR site. (b) shows the wavy TEC perturbations observed by all five receivers during 17:00 – 18:00 UT (00:00 – 01:00 LT) on 11 August 2019.

TEC perturbations shown in Figure 1b are associated with FAIs structures generated near the magnetic equator during 18:30 – 23:00 UT (1:30-5:00 LT), as confirmed by the EAR radar observations.

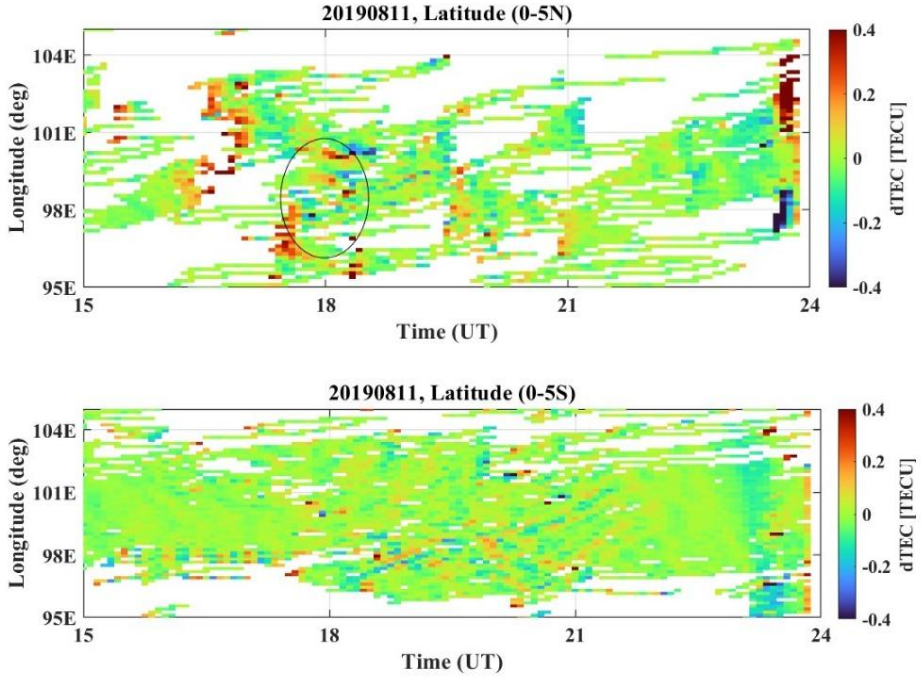

Figure 2: (a) TEC perturbations at a fixed northern latitude as a function of longitude and time. The eclipse shows the northeastward wavy propagation (b) TEC perturbation at a fixed southern latitude.

Furthermore, DTEC maps for the same day were generated to examine the horizontal structures of the TEC perturbations. To investigate their propagation characteristics, TEC perturbations at a fixed latitude were analyzed. The wave structures were found to propagate northeastward during 17:00 -18:00 UT (00:00 – 01:00 LT) as shown in Figure 2(a). These TEC perturbations require further detailed investigation. Therefore, the wavelike TEC perturbations associated with the FAI structures will be discussed in a future publication.

In addition to my research work, I also had the chance to visit the MU Observatory in Shigaraki, a beautiful land of ceramics, with Professor Otsuka. I have seen the Middle and Upper Atmosphere (MU) radar. It spans a vast area and consists of 475 Yagi antennas. The period of my stay at ISEE was 90 days (from July 1 to September 27, 2025) under the guidance of Dr. Yuichi Otsuka, which provided me with a valuable opportunity to collaborate on research problems and exchange scientific ideas. I sincerely thank Dr. Kazuo Shiokawa, Director of ISEE, for providing me with this wonderful opportunity to participate in the program. I would also like to thank Ms. Sayaka Fujiwara for her administrative assistance. I truly enjoyed my stay in Japan - the people, the places, and the food.

(Form11-1)

Power Line Harmonic Radiation Observed by the PWING Network

Kristýna Drastichová; Charles University, Prague, Czech Republic; PhD student

1) Purpose of the Research

We aimed to investigate power line harmonic radiation (PLHR), a type of electromagnetic emission generated by electric power grids at a fundamental frequency (50 or 60 Hz) and their respective harmonics. Although PLHR is normally of low intensity, it can propagate through the ionosphere into the magnetosphere, where it may contribute to radiation belt dynamics.

This work is focused on how geomagnetic activity affects PLHR intensity at different harmonic frequencies. In particular, it aims to understand the role of geomagnetically induced currents (GICs), which are generated during sudden changes in the geomagnetic field on the ground and can affect working conditions of nearby power lines. When the current waveform symmetry is disrupted, PLHR intensity is expected to increase, and even harmonics of the fundamental frequency may appear, which are normally not present. This is important for understanding the effects of space weather on electric power systems on the ground and for their potential monitoring from space.

2) Methods

The research is based on electromagnetic wave measurements obtained by the ground-based PWING network which is operated by ISEE, with Professor Kazuo Shiokawa as P.I. of the PWING project. Since PLHR occurs at well-defined harmonic frequencies, we have performed a custom spectral analysis to obtain power spectral density (PSD) of the measured signals with a fine frequency resolution of 1 Hz and time resolution of 1 s. The PLHR intensity at each harmonic is determined by subtracting the wave background intensities at adjacent frequencies (± 3 Hz).

To be able to characterize geomagnetic activity and estimate the strength of geomagnetically induced currents, magnetometer data near the PWING stations are used. The temporal derivative of the horizontal magnetic field component ($|dB_H/dt|$) with a time resolution of 1 s was utilized as a proxy for GICs magnitude. These local measurements were complemented by geomagnetic indices such as Kp and Dst to provide global insight, as GICs events are thought to be rather local.

3) Results and Discussion

We have successfully prepared custom fine resolution (1 Hz, 1 s) wave data measured by various PWING stations, as outlined in the original proposal. As the PWING network includes many stations worldwide and a large dataset, we initially focused mainly on Finnish power lines, where two PWING

antennas are available, occasionally complemented by the Kannuslehto station for a comparison (Figure 1a). Only data from September 2024 to December 2024 have been used so far, particularly focusing on the 10-11 October 2024 geomagnetic storm. Northern Finland has the advantage of being isolated (a dominant source of PLHR is easier to determine), with power lines extending far north, where GIC events are expected to be strongest (Figure 1b). We have also briefly analyzed data from Canada, which is similarly sparsely populated but has a somewhat different power network configuration.

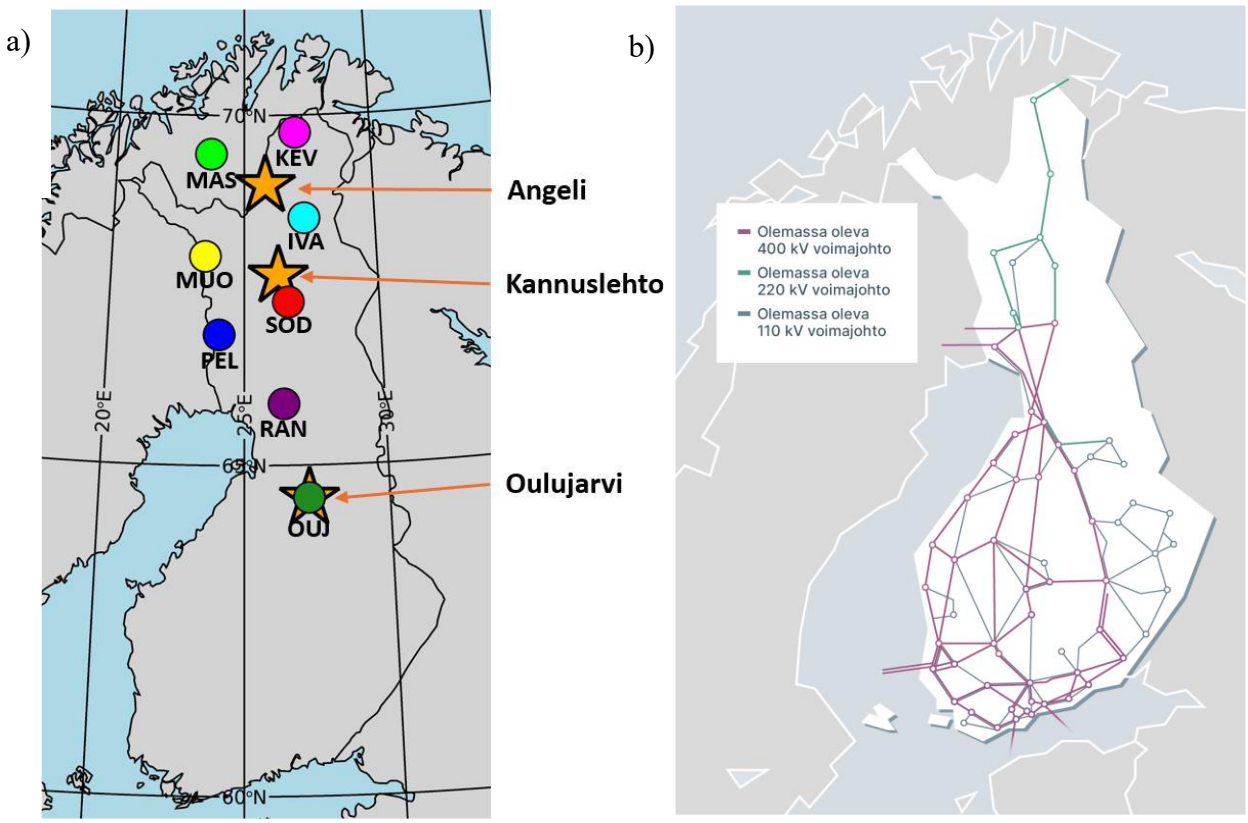

Figure 1: (a) Map of the Finnish power grid; (b) PWING VLF antennas (depicted by a star) and IMAGE network magnetometers (depicted by a circle).

In frequency-time spectrograms, PLHR appears as horizontal lines at its fundamental and harmonic frequencies. Figure 2 shows an example of one-day measurements from the Angeli and Oulujarvi stations during the geomagnetic storm on October 10, 2024. The frequency range analyzed is up to 800 Hz and the X-axis corresponds to universal time (UT). PLHR lines are spaced by 50 Hz. Both odd and even harmonics are visible, with the odd ones being slightly more intense. The Oulujarvi data appear noisier than those from Angeli, which may be because power lines near Oulujarvi are partly buried underground, and the station is located closer to more populated areas. This might make the analysis of the Oulujarvi data more challenging.

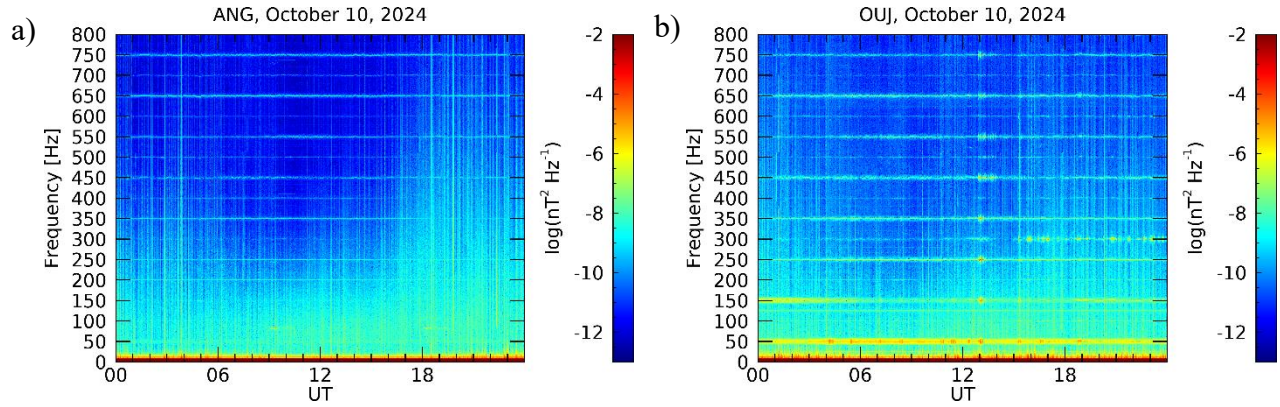

Figure 2: Measured wave intensities by (a) Angeli and (b) Oulujarvi stations during October 10, 2024 geomagnetic storm.

Figure 3 shows a plot in the same format as Figure 2, with the power spectral density (PSD) measured by the Kapuskasing station in northern Canada. The figure includes data from both geomagnetically quiet conditions on October 1, 2024, and the geomagnetic storm on October 10, 2024. In contrast, Figure 2 depicts data from stations in northern Finland during the same storm. The working frequency of the Canadian power grid is 60 Hz, and PLHR lines in the respective spectrograms are spaced by those 60 Hz. The lines corresponding to odd harmonics are much more intense and broader than those at even harmonic frequencies, both during quiet and disturbed conditions. Both spectrograms in Figure 3 are qualitatively similar.

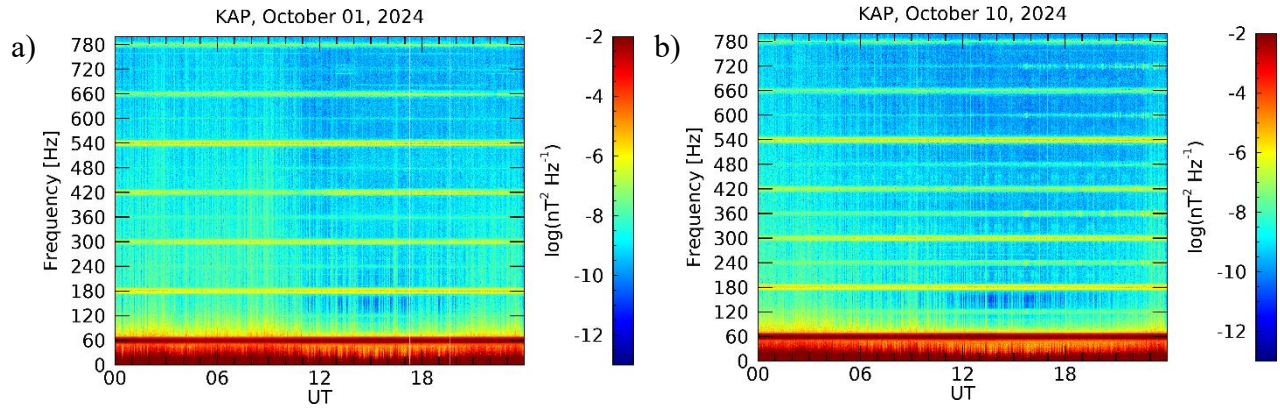

Figure 3: Wave intensities measured by Kapuskasing during (a) geomagnetically quiet time on October 1, 2024 and (b) during geomagnetic storm on October 10, 2024.

Average PLHR intensities measured by the Angeli station from September 2024 to December 2024 are shown in the Figure 4 as a function of a given harmonic frequency and local time (LT). The frequency axis includes only the exact PLHR harmonic frequencies (integer multiples of the fundamental frequency, 50 Hz) and extends up to 1500 Hz. PLHR is much stronger at odd harmonics, with particularly high intensities at 50 Hz, 150 Hz, and 350 Hz, while even and higher-frequency harmonics are much weaker, except for 1050 Hz and 1350 Hz. There is no visible dependence of PLHR intensity on local time.

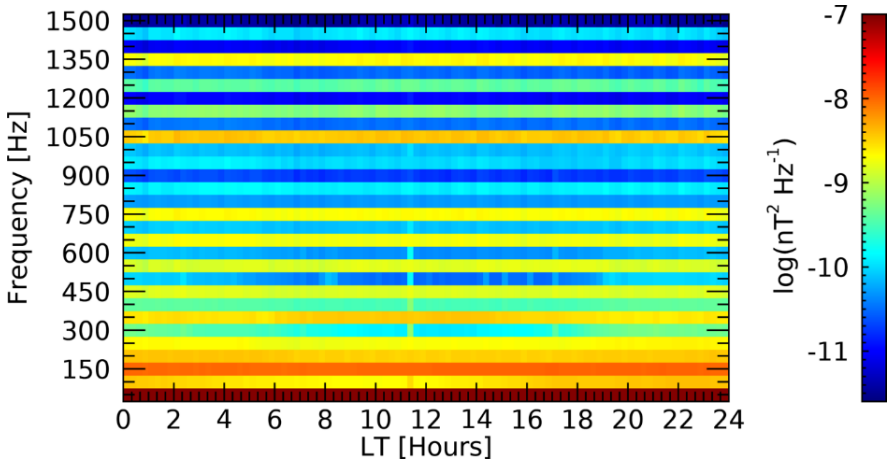

Figure 4: Frequency-local time spectrogram showing the average intensity of PLHR at individual harmonics of the base frequency.

Whether GIC events in northern Finland occur locally or across a wider area is illustrated in Figure 5, where we compare the temporal variations of the horizontal (H) and East–West (Y) components of the measured geomagnetic field. The dataset again spans from September 2024 to December 2024 to allow direct comparison with the wave data obtained by the PWING stations Angeli and Oulujarvi. The locations of the magnetometers are shown in Figure 1a. Quantitatively, the $|dB_X/dt|$ component is typically stronger than $|dB_Y/dt|$ due to the usual orientation of ionospheric electrojets, and the results for $|dB_X/dt|$ are thus very similar to those for $|dB_H/dt|$, so we do not show them separately here. However, the geomagnetically induced currents (GICs) affecting the power systems depend on the local configuration of the network and its orientation relative to the magnetic field change, hence the direction of the variation in geomagnetic field should be considered. Qualitatively, the results for $|dB_H/dt|$ are almost identical for all the 8 magnetometers, with a small exception of the MUO magnetometer where the magnitude exceeded the rest. The same pattern applies for $|dB_Y/dt|$. When we compare the position and the relative magnitude of all the peaks in $|dB_H/dt|$ and $|dB_Y/dt|$, they differ. Note that for a direct comparison, it is better to use magnetic field data with the same 1 s resolution as the wave data; however, in Figure 5 we use hourly averages.

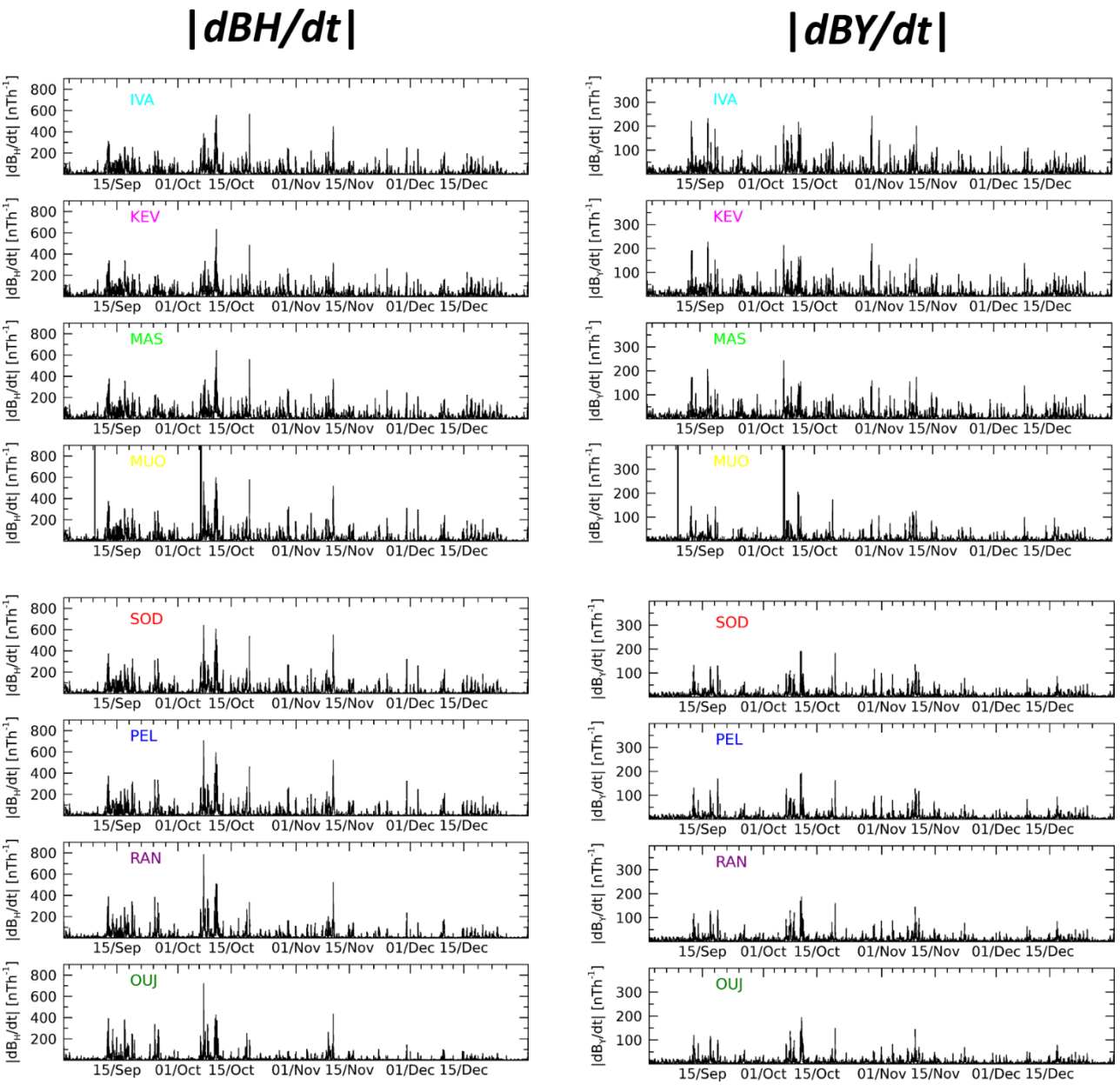

Figure 5: Four months of data from eight IMAGE magnetometers located in northern Finland, with a time resolution of 1 hour, for $|dB_H/dt|$ and $|dB_X/dt||$. Exact locations of magnetometers (IVA, KEV, MAS, MUO, SOD, PEL, RAN and OUJ) are depicted in the Figure 1a.

4) Conclusions

We prepared a preliminary high-resolution wave dataset measured by multiple PWING stations from September 2024 to December 2024, with a particular focus on data from the Angeli and Oulujarvi stations. We also analyzed in more detail a large geomagnetic storm that occurred on October 10-11, 2024. Even harmonics of PLHR were observed during both storm-time and quiet conditions, although they were generally weaker.

The analysis of the average wave intensities measured by the Angeli station shows that PLHR is strongest at its fundamental frequency and then at lower odd harmonics, as well as at 1050 Hz and 1350 Hz. No clear dependence of PLHR intensity on local time was found.

The analysis of data from the IMAGE magnetometer network in northern Finland suggests that it may be important to study PLHR intensities not only with respect to $|dB_H/dt|$, but also with respect to variations in individual components of the magnetic field.

Currently, we are examining how PLHR intensity statistically depends on $|dB_H/dt|$, $|dB_X/dt|$, and $|dB_Y/dt|$ using a larger dataset that includes more geomagnetic storms and additional PWING stations, and performing PLHR propagation analysis to determine the possible source location

5) Periods of stay

September 23, 2025 – December 11, 2025

6) List of publications

(*Connected to my SCOSTEP stay)

- Drastichová, K., Němec, F., Shiokawa, K., Martinez-Calderon, C., Manninen, J., Raita, T., Power Line Harmonic Radiation Observed by the PWING Network (P), SGEPSS 2025 Fall Meeting, Kobe, Japan, 24-27 November, 2025.

Project Title:

Thermospheric and Ionospheric Perturbations at Mid-Latitudes during Solar Maximum : Implications for Space Weather.

Principal Investigator Name (Affiliation) :

Thomas LHEUREUX, research institute of astrophysic and planetology (IRAP, Toulouse, France), PhD student.

Thomas.lheureux@riap.omp.eu

Introduction and purpose :

My PhD thesis focuses on observations of the thermosphere (≈ 90 km to ≈ 500 km) and the ionosphere (≈ 80 km up to the exosphere) through airglow. Airglow is a natural phenomenon that corresponds to the de-excitation of atoms and molecules in the upper atmosphere. The Sun continuously emits particles and radiation, which are absorbed by atoms and molecules in the Earth's atmosphere on the dayside. At night, when ultraviolet radiation is no longer present, these atoms and molecules return to their ground states by emitting photons, giving rise to airglow.

This method is particularly useful because it allows access to parameters of the thermosphere that are otherwise difficult to measure. The thermosphere is predominantly a neutral medium, which limits studies involving electric or magnetic fields. Moreover, the low density of the thermosphere prevents the use of balloon-borne probes, although it remains to dense for satellites to maintain orbit consistently.

Focusing now on the application of airglow: when a Coronal Mass Ejection (CME) or a solar eruption occurs, charged particles from the Sun enter the Earth's atmosphere. These particles are redirected by the Earth's magnetic field along magnetic field lines toward the magnetic poles. In the process, they transfer energy to the atmosphere via Joule heating, raising its temperature and generating gravity waves (GWs). These wave-like structures propagate toward the equator. Gravity waves propagate similarly to sound waves, creating regions of higher density of neutral atoms and molecules. Under quiet conditions, airglow is expected to be homogeneous but during geomagnetic storms, these higher-density regions enhance the airglow (see fig.1). This enhancement allows us to determine various parameters, such as the propagation speed and wavelength of the waves.

The aim of my PhD is to conduct this type of study while demonstrating that it can be performed using low-cost equipment. Specifically, I am using three ZWO ASI cameras (≈ €2000 each) equipped with three different filters to probe various altitudes. At each altitude, different atoms and molecules are present, each with distinct energy levels, and the filters allow us to selectively observe specific atmospheric layers.

My PhD supervisor contacted Pr. Kazuo Shiokawa after a conference on this topic, who have extensive experience conducting research with this type of equipment. I visited ISEE and Professor Kazuo Shiokawa's team from February 6 to June 30, 2025, to receive training on camera installation, operation, and data interpretation.

Methods :

During my stay, we primarily focused on the fundamentals of airglow imaging, which included :

1) The installation of cameras.

2) Understanding the routine for acquiring continuous images thoughout the night.

3) Initial step into image processing.

Results :

(1) To properly install the cameras, it is essential to consider that they will operate every night. This requires protecting the equipment to ensure long-term durability and to obtain high-quality images. Our plan is to install a set of three cameras that can be remotely operated. We aim to develop a reproducible structure that can be easily implemented at multiple sites to facilitate research activities.

We concluded that the structure should consist of two parts : an upper section with a fully hermetic dome, from which only the three camera objectives protrude, and a lower section beneath the dome housing the computers and cameras. Thermal insulation is necessary to maintain a stable temperature, preventing variations in the CCD performance. Humidity is also a concern, as it can damage the equipment and cause condensation on the dome, potentially rendering observations unusable. Ventilation will be added to mitigate this issue.

Since the initial installation is planned at Pic du Midi in the Pyrénées (2 877m), France, we decided that a cylindrical shape would be most suitable to prevent snow accumulation on the structure. The preliminary design of this setup is presented in Fig. 2

(2) Since Professor Kazuo Shiokawa and his team have extensive experience with this type of camera, they kindly provided me with the routine they use to acquire continuous airglow images throughout the night. I spent just over a week studying the code in detail and consulted with Yuka Yamamoto, who developed it. Depending on the filter used, different exposure times are required to obtain usable images, as the emission rate varies across atmospheric layers. I also learned the key parameters needed to acquire comparable images, ensuring that our observations can be reliably compared with those of Professor Shiokawa's team.

(3) Finally, I moved on to data processing. The first task I completed was translating an IDL code into Python. This code is essential for all subsequent analyses, as it allows us to determine the zenith position in an astronomical image. Knowing the zenith enables us to rotate the image so that north is oriented upward, which facilitates direct comparison between different filters. In other words, even if the cameras are not initially aligned in the same direction, we can still rotate the images to observe the same event without difficulty, ensuring consistency across datasets. This code uses two stars in the image, whose right ascension and declination are known, to relate their actual angular positions to their positions in the image (pixels), allowing for the precise determination of the zenith in the image.

I then finally began developing a code to process the data and prepare it for analysis. This includes removing stars from the images, subtracting the contribution of the Milky Way, correcting for optical artifacts (via calibration), and minimizing the effects of light pollution. Natural effects, such as atmospheric extinction and the Van Rhijn effect—which causes higher

apparent brightness near the horizon due to the increased air mass—are also corrected. Combined with dark frames and flat-field corrections, the observations are now fully calibrated and ready for scientific analysis.

Unfortunately, the structure is not yet fully operational (it may be ready within the next few months), so I am currently unable to present images from this work. However, if you are interested in this study, please feel free to contact me by email.

Fig. 1 - Airglow at Pic du Midi, France. Denser region emmits more airglow light resulting with these greens parallel lines**.**

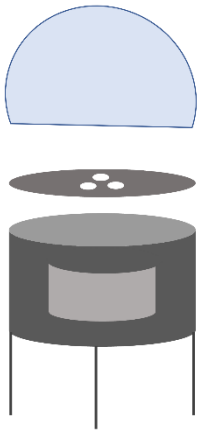

Fig. 2 – Structure for ZWO cameras. First version, work is still in progress, the structure should be ready soon.

Name: Manar Gamal
Affiliation: Egypt-Japan University of Science and Technology (E-JUST)

Report on Stay at the Institute for Space-Earth Environmental Research (ISEE), Nagoya University

I had the great opportunity to spend three months at the Institute for Space-Earth Environmental Research (ISEE), Nagoya University, Japan, as a visiting scholar funded by the SCOSTEP Visiting Scholar (SVS) Program, from 1 Oct. to 27 Dec. This experience was both academically enriching and personally memorable, allowing me to develop my research skills while experiencing a new culture and environment.

My primary focus during the stay was conducting research on muon bundles and their applications in muography, particularly for detecting and monitoring tectonic plate movements in Japan, under the supervision of Dr. Menjo. This research involved generating air shower simulations using the COSMOS framework and analyzing the resulting data using ROOT and Python to study muon density, distribution, and timing characteristics. The work is currently ongoing and is expected to lead to a scientific publication, while also contributing to the development of an extended research collaboration in this field.

One of the highlights of my stay was visiting the Earthquake Research Institute at the University of Tokyo with Dr. Menjo. During this visit, we met with Prof. Akimichi Taketa and had the opportunity to visit an observation site, where I learned about important geological phenomena and observed the borehole detector. This experience provided valuable insight into how muography can be applied in real-world geophysical studies, particularly in earthquake-related research.

Outside of my academic activities, I had the chance to explore Japan and experience its rich culture. In Nagoya, I visited several historical and touristic sites and enjoyed trying a variety of Japanese foods. I also traveled to Hamamatsu, where I spent time by the ocean. In addition, I explored important sites in Tokyo and had the opportunity to see Mount Fuji, which was one of the most memorable experiences of my stay.

I would like to express my sincere gratitude to Dr. Menjo for his continuous support, guidance, and encouragement throughout my stay. I am also very thankful to Ms. Sayaka Fujiwara and Ms. Mai Asukra for their kind assistance. My appreciation also goes to Yoko and Karina from the residency office for their help with

accommodation and logistics. Special thanks to Ms. Kato Waka and my colleagues at the Cosmic Ray Department office for their support and for creating a welcoming and collaborative environment.
I would also like to sincerely thank all ISEE members for their kindness, friendliness, and warm hospitality throughout my stay.

Fabry-Perot Observations of Thermospheric Winds and Their Response to a Geomagnetic Storm Event

Researcher: Arthur Gauthier, DLR, PhD
Host Institution: Institute for Space-Earth Environmental Research, Nagoya University
Home Institution: DLR German Aerospace Center, Neustrelitz
Supervisors: Claudia Borries, Gunter Stober
Host Supervisor: Shin-ichiro Oyama
Period of Stay: 04 November 2025- 19 December 2025

Purpose:

Thermospheric winds play a key role in the redistribution of energy and momentum in the upper atmosphere and strongly influence ionospheric dynamics. Accurate measurements are therefore essential for improving space weather modelling and mitigating impacts on satellite operations and communication systems.
This project had two main objectives:
(1) to validate and compare wind retrieval methods applied to Fabry–Pérot Interferometer (FPI) observations, focusing on the newly installed SOFPIT instrument in Tenerife; and
(2) to investigate the thermospheric wind response to the geomagnetic storm of 10 May 2024.

Methods:

Thermospheric winds were derived from FPI observations of the 630.0 nm atomic oxygen airglow emission (200–300 km altitude). The dataset includes measurements from SOFPIT (Tenerife) and ISEE FPI at Tromsø/Skibotn. The analysis was performed using Python-based tools.
For the SOFPIT instrument in Tenerife, two retrieval methods were applied. The opposite-direction method (Shiokawa et al., 2012) estimates winds by comparing line-of-sight measurements in opposite viewing directions. In addition, a forward modelling approach (Makela et al., 2011) was used to retrieve wind and temperature through inversion, assuming zero vertical wind over a night. For the FPI in Tromsø/Skibotn, wind retrieval is performed using the opposite-direction method.

Results:

<u>Instrumentation and Retrieval Comparison:</u>

The SOFPIT and Tromsø/Skibotn FPIs differ mainly in their etalon design. SOFPIT uses a fixed-gap etalon, providing higher stability and simpler calibration. In contrast, the Tromsø/Skibotn instrument employs a large-aperture (116 mm) tunable-gap etalon, offering higher spectral resolution and sensitivity but increased mechanical and thermal variability, as the gap depends on environmental conditions and is monitored via fringe positions. Both systems use CCD detectors and sky scanners for multi-directional observations.
Differences are also present in the retrieval methods. For SOFPIT, both the Shiokawa and a forward-model-based method were applied. In both cases, the center determination using laser images and azimuthal averaging with Gaussian fitting is identical. The Tromsø/Skibotn FPI, however, uses a different center-finding

approach based on Gaussian fits across multiple image slices, while keeping a similar averaging and peak detection procedure. These differences affect the sensitivity of the retrieved winds to instrumental and atmospheric assumptions.

Storm-Time Wind Dynamics (10 May 2024):

A clear intensification of thermospheric winds is observed during the geomagnetic storm compared to the preceding nights (7–9 May). Under quiet conditions, zonal and meridional winds remain within approximately ±100 m/s. During the storm, zonal winds increase significantly, reaching up to around 300 m/s in the westward direction. Meridional winds show a similar enhancement, with strong equatorward flows exceeding 300 m/s. In addition, the storm-time winds exhibit increased variability and multiple directional reversals throughout the night. These results demonstrate a strong thermospheric response to geomagnetic forcing, consistent with enhanced energy input and disturbed global circulation.

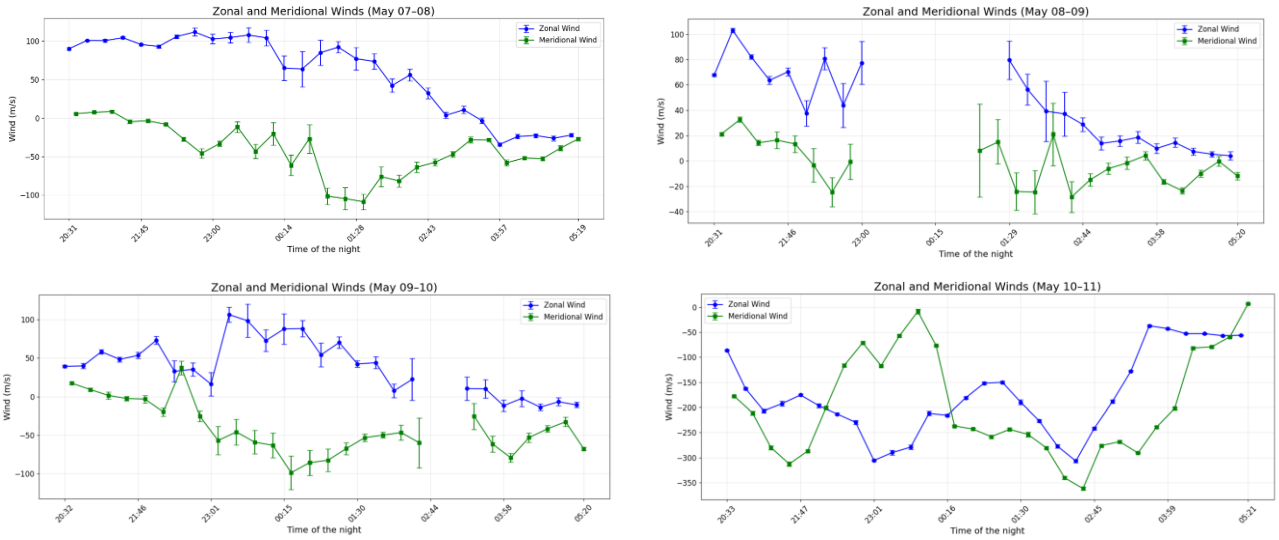

Figure 1: *S*OFPIT zonal (top) and meridional (bottom) winds for 7–11 May 2024

Exploratory Geophysical Analysis:

An additional exploratory study was initiated using the GeospaceLab framework, enabling combined analysis of multi-instrument data such as OMNI solar wind parameters, GNSS TEC, and GRACE-FO winds.

The aim was to investigate the generation and propagation of large-scale travelling ionospheric disturbances (LSTIDs). Although preliminary, this approach provides a basis for future global-scale studies.

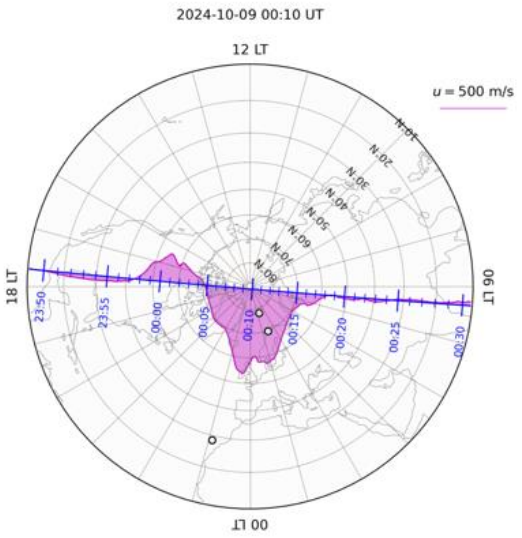

Figure 2: Cross-track zonal neutral winds from GRACE-FO, visualized using GeospaceLab